Steffens, L.M., Díez, P., A simple strategy to assess the error in the numerical wave number of the Finite Element solution of the Helmholtz equation, *Computer Methods in Applied Mechanics and Engineering*, Vol. 198, Issues 15-16, pp. 1389-1400, 2009

A simple strategy to assess the error in the numerical wave number of the Finite Element solution of the Helmholtz equation

Lindaura Maria Steffens and Pedro Díez *

Laboratori de Càlcul Numèric, Departament de Matemàtica Aplicada III
Universitat Politècnica de Catalunya,
Mòdul C2, Jordi Girona 1-3, Barcelona E-08034, Spain

Abstract

The standard approach for goal oriented error estimation and adaptivity uses an error representation via an adjoint problem, based on the linear functional output representing the quantity of interest. For the assessment of the error in the approximation of the wave number for the Helmholtz problem (also referred to as dispersion or pollution error), this strategy cannot be applied. This is because there is no linear extractor producing the wave number from the solution of the acoustic problem. Moreover, in this context, the error assessment paradigm is reverted in the sense that the exact value of the wave number, κ, is known (it is part of the problem data) and the effort produced in the error assessment technique aims at obtaining the numerical wave number, κ_H, as a postprocess of the numerical solution, u_H. The strategy introduced in this paper is based on the ideas used in the a priori analysis. A modified equation corresponding to a modified wave number κ_m is introduced. Then, the value of κ_m such that the modified problem better accommodates the numerical solution u_H is taken as the estimate of the numerical wave number κ_H. Thus, both global and local versions of the error estimator are proposed. The obtained estimates of the dispersion error match the a priori predicted dispersion error and, in academical examples, the actual values of the error in the wave number.

Key words: Wave problems; Helmholtz equation; Error estimation of wave number; Dispersion/pollution error; Goal-oriented adaptivity; Global/local estimates

⋆ Partially supported by Ministerio de Educación y Ciencia, Grants DPI2007-62395 and BIA2007-66965;Programme Alβan, the European Union Programme of High Level Scholarships for Latin America, scholarship n^o E06D100641BR

* Corresponding author.
Email addresses: lindaura.steffens@upc.edu (Lindaura Maria Steffens), pedro.diez@upc.edu (Pedro Díez).
URL: http://www-lacan.upc.edu (Pedro Díez).

1 Introduction

The numerical simulation of acoustic problems requires an accurate answer to properly predict their performance. In the low frequency range domain the Finite Element Method (FEM) is a standard tool for solving the acoustic equations. In the medium and high frequency ranges the end-user should be concerned by the errors associated with the numerical discretization. In practice, two components of the error are clearly identified in this framework: interpolation error and pollution error. The classical interpolation error decays with the mesh size as predicted by standard a priori error estimates. The behavior of the pollution error is more complex: the convergence rate predicted by the a priori estimates depends on the range where the mesh size lies (relative to the wavelength) [1].

In practice, the end-user of a Finite Element acoustic computation is concerned with the accuracy of the solution in terms of the dispersion, the error committed in the evaluation of the wave number, κ. Paradoxically, this is not because the value of κ is a quantity of interest that has to be evaluated accurately. In fact, the exact value of κ is known a priori as part of the problem data. The overall quality of the numerical solution is however associated with the error in the approximation of κ.

The standard approach for goal oriented error estimation and adaptivity is based on the representation of the error in a quantity of interest obtained using an adjoint problem [14,17]. The solution of the adjoint problem is also denoted extractor and the corresponding error representation combines the extractor and the original solution. Thus, the error assessment for the quantity of interest is reduced to assess the error in energy norm of this auxiliary problem. This strategy cannot be used when the quantity to be assessed is the wave number. This is because there is not a proper extractor associated with this quantity, κ. Moreover, as already noted, the exact value of κ is a priori known. This reverts the final goal of the error assessment technique. The target of the error estimation strategies is in standard cases to find a better approximation than the one provided by the numerical solution, u_H, and then compare them. In the present situation, this is somehow reverted to find the actual approximation of the quantity of interest provided by u_H, say κ_H, and to compare it with the exact value κ. Summarizing, assessing the error in κ requires a complete different paradigm. The quality of the solution is assessed via the approximation of a quantity which is exactly known. The numerical wave number κ_H is unknown and has to be evaluated.

The first problem to face is to find a proper definition for κ_H. Heuristically, the *wavelength* of the approximate solution is the distance of two consecutive local maxima (or minima). Although this represents a precise definition for 1D waves, it cannot be easily generalized to higher dimensions. Moreover, it cannot be converted into an explicit functional output of the numerical solution. One definition for κ_H is implicitly used in a priori analysis, based on the idea of fitting the numerical

solution into a modified equation. Here, this concept is extended such that it can be exploited in a posteriori error assessment setting.

Namely, this paper introduces a technique to assess the value of κ_H based on finding the wave number of a modified problem which better accommodates the numerical solution u_H. This approach is inspired by the a priori estimates developed in [12].

The idea is also extended to find a local indicator of the error in the wavelength. This local quantity is assumed to measure the ability of the local discretization (in a given portion of the domain) to properly capture the wavelength. The possible use of this information to adapt the mesh and reduce the overall error is beyond the scope of this paper but is part of the work in progress.

The remainder of the paper is structured as follows. Section 2 introduces the notation presenting the problem to be solved, the Finite Element formulation and the concepts of dispersion and pollution effect in this type of problem. The basic lines of the a priori analysis performed in [12] are briefly sketched in section 3. Then, section 4 is devoted to introduce the a posteriori technique proposed to assess the error in the wave number. A local version of the estimate providing a spatial error distribution for adaptive purposes is introduced in section 5. Finally, section 6 contains numerical examples showing the good behavior of the proposed technique both in academic and practical examples.

2 Problem statement

2.1 Acoustic modeling: the Helmholtz equation

The presentation and notation introduced by Ihlenburg [11] is followed in the remainder of this section.

The transient acoustic problem consists in obtaining the unknown pressure field $P(\mathbf{x}, t)$, taking values for $\mathbf{x} \in \Omega \subset \mathbb{R}^d$ (d being the dimension in space, d =1, 2 or 3). The field $P(\mathbf{x}, t)$ is the solution of the following partial differential equation

$$\Delta P = \frac{1}{c^2} \frac{\partial^2 P}{\partial t^2}, \tag{1}$$

where c is the speed of sound in the medium.

The pressure time dependency is eliminated assuming a harmonic behavior and selecting an angular frequency ω, namely

$$P(\mathbf{x}, t) = u(\mathbf{x}) \exp(i\omega t) \tag{2}$$

where $u(\mathbf{x})$ is the complex spatial distribution of the acoustic pressure and i the imaginary unit. Substituting (2) into (1), the wave equation reduces to the Helmholtz equation:

$$\Delta u + \kappa^2 u = 0 \tag{3}$$

where $\kappa := \omega/c$ stands for the wave number.

The physical pressure is the real part of the complex unknown u. The velocity $\mathbf{v}$ is proportional to the gradient of pressure:

$$\nabla u = -i\rho c\kappa \mathbf{v} \tag{4}$$

where ρ is the density of the fluid.

A complete definition of the Boundary Value Problem to be solved requires adding to equation (3) a proper set of boundary conditions. For interior acoustic problems, three types of boundary conditions are considered: Dirichlet, Neumann and Robin (or mixed).

The Dirichlet boundary conditions prescribe values of the pressure on part of the boundary, say $\Gamma_D \subset \partial\Omega$, where u is prescribed to be equal to a given value $\bar{u}$, that is

$$u = \bar{u} \ \text{ on } \ \Gamma_D. \tag{5}$$

On the Neumann part of the boundary $\Gamma_N \subset \partial\Omega$ the normal component of the velocity $\mathbf{v}$ is prescribed to be equal to $\bar{v}_n$, namely

$$\frac{\partial u}{\partial \mathbf{n}} = -i\rho c\kappa \bar{v}_n \ \text{ on } \ \Gamma_N. \tag{6}$$

The prescribed value $\bar{v}_n$ corresponds to the normal velocity of a vibrating wall producing the sound that propagates within the medium.

Finally, on the Robin part of the boundary $\Gamma_R \subset \partial\Omega$ the velocity is imposed to be proportional to the pressure, that is

$$\frac{\partial u}{\partial \mathbf{n}} = -i\rho c\kappa A_n u \ \text{ on } \ \Gamma_R, \tag{7}$$

where the coefficient A_n is the admittance and represents the structural damping. This type of boundary conditions is associated with absorbing walls. For $A_n = 0$ it coincides with the homogeneous Neumann boundary condition, standing for a perfectly reflecting panel. For particular case of plane waves, the value $A_n = 1/\rho c$ describes a fully absorbent panel.

In order to get a well posed Boundary Value Problem, the three parts of the boundary must cover the whole boundary, that is $\partial\Omega = \overline{\Gamma_D \bigcup \Gamma_N \bigcup \Gamma_R}$.

The weak form of the Boundary Value Problem defined by equations (3), (5), (6) and (7) is readily expressed in its weak form using the corresponding natural func-

tional spaces. The space for the trial functions is $U = \{u \in \mathrm{H}^1(\Omega), u|_{\Gamma_D} = \bar{u}\}$ while the space for the test functions is $V = \{v \in \mathrm{H}^1(\Omega), v|_{\Gamma_D} = 0\}$, $\mathrm{H}^1(\Omega)$ being the standard Hilbert space of square integrable functions with square integrable first derivatives.

Thus, the weak form of the problem reads: find $u \in U$ such that

$$a(u, v) = l(v), \quad \forall v \in V, \tag{8}$$

where the bilinear and linear forms are defined as follows

$$\begin{aligned} a(u, v) &:= \int_\Omega \nabla u \cdot \nabla \tilde{v} \, d\Omega - \int_\Omega \kappa^2 u \tilde{v} \, d\Omega + \int_{\Gamma_R} i\rho c\kappa A_n u \tilde{v} \, d\Gamma \\ \text{and } l(v) &:= -\int_{\Gamma_N} i\rho c\kappa \bar{v}_n \tilde{v} \, d\Gamma, \end{aligned}$$

and the symbol $\tilde{\cdot}$ denotes the complex conjugate.

2.2 Finite Element approximation

The discrete counterparts of U and V are the finite element spaces $U_H \subset U$ and $V_H \subset V$ associated with a mesh of characteristic element size H. Thus, the discrete finite element solution is the function $u_H \in U_H$ such that

$$a(u_H, v_H) = l(v_H) \ \ \forall v_H \in V_H. \tag{9}$$

The finite element solution u_H is expressed in terms of the basis-functions N_j spanning U_H:

$$u_H = \sum_{j=1}^{n} N_j u_j = \mathbf{N}\mathbf{u}_H, \tag{10}$$

where u_j, for $j = 1, 2 \ldots n$, are the complex nodal values, $\mathbf{N} = [N_1, N_2 \ldots N_n]$ and $\mathbf{u}_H^{\mathsf{T}} = [u_1, u_2, \ldots, u_n]$

The matrix form of (9) reads

$$(\mathbf{K}_H + i\rho c\kappa A_n \mathbf{C}_H - k^2 \mathbf{M}_H)\mathbf{u}_H = -i\rho c\kappa \mathbf{f}_H, \tag{11}$$

where $\mathbf{K}_H$, $\mathbf{C}_H$ and $\mathbf{M}_H$ are the so-called stiffness, damping and mass matrices defined by

$$\mathbf{K}_H := \int_\Omega (\nabla \mathbf{N})^{\mathsf{T}} (\nabla \mathbf{N}) \, d\Omega, \quad \mathbf{C}_H := \int_{\Gamma_R} \mathbf{N}^{\mathsf{T}} \mathbf{N} \, d\Gamma \ \text{ and } \ \mathbf{M}_H := \int_\Omega \mathbf{N}^{\mathsf{T}} \mathbf{N} \, d\Omega \, .$$

Note that the damping matrix $\mathbf{C}_H$ accounts for the Robin boundary conditions while the right-hand side term vector $\mathbf{f}_H$ given by

$$\mathbf{f}_H := \int_{\Gamma_N} \mathbf{N}^\mathsf{T} \bar{v}_n \, d\Gamma$$

includes the effect of Neumann boundary conditions.

2.3 Dispersion and Pollution effects

The error introduced in the numerical solution of wave problems has two different components: *interpolation error* and *pollution error*. The interpolation error is the classical error arising in elliptic problems and pertains to the ability of the discretization to properly approximate the solution. The interpolation error is obtained by simply using the exact values of u at the mesh nodes $\mathbf{x}_j$, $j = 1, 2 \ldots n$:

$$\text{Interpolation error } = u(\mathbf{x}) - \sum_{j=1}^{n} N_j(\mathbf{x}) u(\mathbf{x}_j)$$

In standard thermal and elasticity problems (i.e problems for which the bilinear form $a(u, v)$ in 8 is symmetric as positive-definite, that is, induces an inner product), the error in the finite element solution is equivalent to the interpolation error, and converges with the same rate. This error is local in nature because it may be reduced in a given zone by reducing the mesh size locally in this zone.

In wave problems, in particular in the solution of the Helmholtz equation, a new error component has to be considered which is referred to as *pollution* error. This error component is especially relevant in the framework of Helmholtz problems due to the blowup of the inf-sup and continuity constants of the weak form when the wave number is large (i.e. the inf-sup constant tends to zero and the continuity constant tends to ∞ as κ tends to ∞). In transient wave problems, pollution is associated with the variation of the numerical wave speed with the wavelength. This phenomenon results in the dispersion of the different components of the total wave. In the steady Helmholtz problem, the word dispersion is also used and corresponds to the error in the numerical wave number, κ_H, and it is therefore identified with the pollution. In other words, the FE error is decomposed into two terms which, in the case of wave problems, behave completely differently:

$$\text{FE error } = u(\mathbf{x}) - \sum_{j=1}^{n} N_j(\mathbf{x}) u_j = \text{ Interpolation error } + \underbrace{\sum_{j=1}^{n} N_j(\mathbf{x})(u(\mathbf{x}_j) - u_j)}_{\text{dispersion/pollution}} .$$

This is illustrated in Figure 1. The second term in this estimate characterizes the pollution error and is denoted by e_{pol}. This error component is related to the phase

difference between the exact and FE solutions, that is the dispersion.

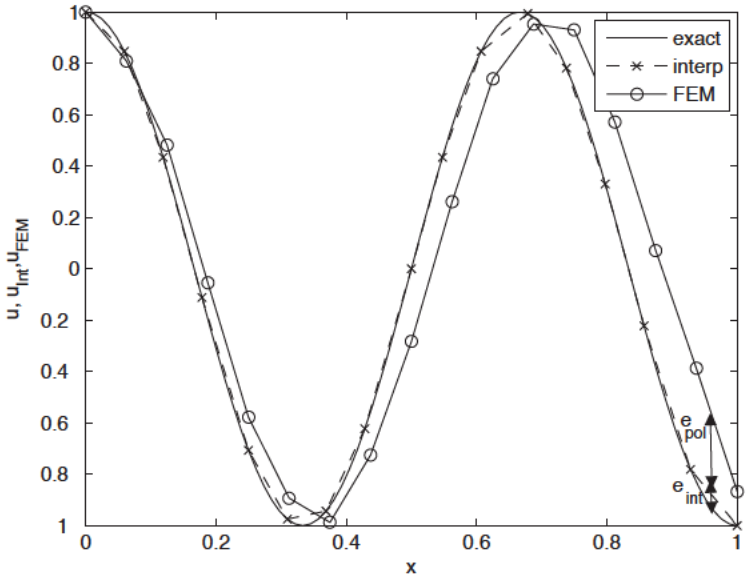

Fig. 1. Illustration of the errors arising in the approximation of the Helmholtz equation. The exact solution (solid line, smooth) and interpolant (dashed line) coincide at the nodes, the FEM solution reproduces approximately the shape of the wave with a larger wavelength ($\kappa_H < \kappa$).

Much attention has been paid to the a priori analysis of the pollution/dispersion error, see for instance [4,12,13]. As shown in section 3, the pollution term converges at a different rate, lower than the standard interpolation error. The pollution effect may be suppressed only in 1D problems, as noted in [2,3]. In higher dimensions, pollution affects every numerical scheme and cannot be avoided [4].

3 A priori error assessment

The a priori error analysis is performed studying a simple 1D case [12]. This analysis is recalled here because its basic rationale is useful in the following. The analysis is based on considering a modified problem and identifying the parameter of the modified problem that better accommodates the FE solution.

3.1 Modified problem

A modified Helmholtz equation is introduced as

$$\Delta u_m + \kappa_m^2 u_m = 0. \tag{12}$$

Note that in the 1D case, this reduces to

$$\frac{d^2u_m}{dx^2} + \kappa_m^2 u_m = 0. \tag{13}$$

Therefore, in 1D case, supposing that $\Omega = (0,1)$, the solution $e^{i\kappa_m x}$ is obtained from the characteristic solutions by selecting the following boundary conditions: $u_m(0) = 1$ and $u_m'(1) = i\kappa u(1)$.

The a priori analysis aims at determining the value of κ_m that better accommodates the numerical solution of the Helmholtz equation. This value κ_m is identified with the discrete wave number and it is denoted by κ_H^{pri} (the superscript *pri* stands for *a priori*).

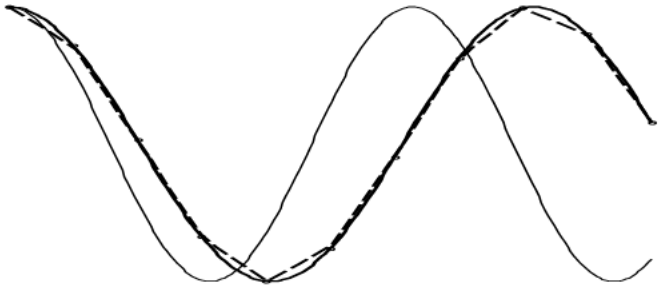

Fig. 2. Illustration for the 1D case of the exact solution u (solid thiner line), the approximate solution u_H (dashed line) and the solution of the modified problem u_m (thicker solid line) for $\kappa_m = \kappa_H^{\text{pri}}$, coinciding with u_H at the nodes.

To this end, the patch of elements surrounding node $\mathbf{x}_j$ in a 1D mesh is considered, see figure 3. Let N_{j-1}, N_j and N_{j+1} be the linear shape functions corresponding to

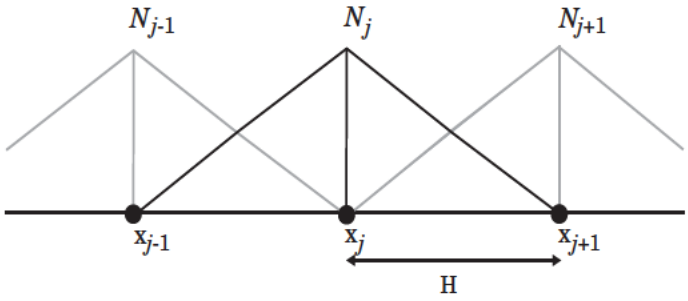

Fig. 3. Nodes surrounding $\mathbf{x}_j$ in a 1D linear FEM mesh and their corresponding shape functions

the nodes $\mathbf{x}_{j-1}$, $\mathbf{x}_j$ and $\mathbf{x}_{j+1}$, which are consecutive in the mesh and are the only ones involved in the equation for node $\mathbf{x}_j$. The discrete equation corresponding to node $\mathbf{x}_j$ reads

$$Ru_{j-1} + 2Su_j + Ru_{j+1} = 0, \tag{14}$$

the coefficients R and S being defined as

$$R := -1 - \frac{1}{6}(\kappa H)^2 \text{ and } S := 1 - \frac{1}{3}(\kappa H)^2$$

and u_j the nodal unknown at node $\mathbf{x}_j$.

Noting that $\mathbf{x}_{j-1} = \mathbf{x}_j - H$ and $\mathbf{x}_{j+1} = \mathbf{x}_j + H$, using $u_m(\mathbf{x}) = e^{i\kappa_m \mathbf{x}}$ and replacing κ_m by κ_H^{pri} in the discrete equation (14) yields the following expression (see [12] for details):

$$\kappa_H^{\text{pri}} H \approx \kappa H - \frac{1}{24}(\kappa H)^3 + O((\kappa H)^5). \tag{15}$$

Consequently, the following a priori estimate for the dispersion error is defines as

$$E^{\text{pri}} := \kappa - \kappa_H^{\text{pri}} \approx \frac{\kappa^3 H^2}{24}. \tag{16}$$

Next section introduces an a posteriori error estimation technique that is inspired by the derivation of the above a priori estimate.

4 A posteriori error estimation of the wave number

The standard approach to obtain an error estimate in some Quantity of Interest (QoI) defined by a linear functional is to obtain an error representation using an adjoint problem. The adjoint problem for linear problems is similar to the direct one but with different *loads* (source term and/or boundary conditions). The error representation is an expression of the error in the QoI as an *energy* product of the errors of the direct and adjoint problems [1].

Recall however that the aim is here to assess the error in the wave number κ, which is the current QoI. The error assessment using an adjoint problem and the corresponding error representation is not applicable for the wave number QoI. This is due to two reasons. First, there is no linear functional extracting the wave number (or the wavelength) of an arbitrary function u. Second, in this case the value for κ is known for the exact solution u (it is an input data!) but not for the numerical solution u_H: κ is known but κ_H is unknown. The strategy of the error estimate is reversed in this case. Instead of devoting effort to obtain a better approximation, as close as possible to the exact solution and then, compare it with the numerical result, here the effort has to be oriented to obtain the wave number of the approximate solution.

A new approach to a posteriori error estimation is introduced here, based on the ideas of the a priori analysis sketched in section 3.

4.1 Direct and inverse solution of a computable modified equation

Recall that, in the a priori analysis, a modified problem is introduced into which the numerical solution can be somehow injected. The same idea is used here in an a posteriori setup. To do that, a computable modified problem has to be defined on a computable basis as it is standard in error estimation procedures [9,15]. To this effect, the exact modified problem is replaced by a reference one, associated with a finer mesh of characteristic element size $h < H$. Thus, the solution of the modified problem is a nodal value vector $\mathbf{u}_m$ (in the finer h-mesh) such that

$$[\mathbf{K}_h + i\rho c A_n \kappa_m \, \mathbf{C}_h - \kappa_m^2 \mathbf{M}_h] \, \mathbf{u}_m = -i\rho c \kappa_m \, \mathbf{f}_h \tag{17}$$

Note that this can also be solved as an inverse problem by considering the solution $\mathbf{u}_m$ as input. Then, for the given $\mathbf{u}_m$ the inverse problem is finding κ_m such that $\mathbf{u}_m$ is the solution of (17). This is performed minimizing the residual norm.

For a given $\mathbf{u}_m$, the residual is defined as a function of the wave number κ_m, that is

$$\begin{aligned} \mathbf{r}(\kappa_m; u_m) &:= [\mathbf{K}_h + i\rho c A_n \kappa_m \, \mathbf{C}_h - \kappa_m^2 \mathbf{M}_h] \, \mathbf{u}_m + i\rho c \kappa_m \, \mathbf{f}_h \\ &= \mathbf{a}_0 + \mathbf{a}_1 \kappa_m + \mathbf{a}_2 \kappa_m^2, \end{aligned} \tag{18}$$

where

$$\mathbf{a}_0 = \mathbf{K}_h \mathbf{u}_m, \;\; \mathbf{a}_1 = i\rho c (A_n \mathbf{C}_h \mathbf{u}_m + \mathbf{f}_h) \;\; \text{and} \;\; \mathbf{a}_2 = -\mathbf{M}_h \mathbf{u}_m.$$

Note that given $\mathbf{u}_m$, the squared residual norm $\mathbf{r}'\mathbf{r}$ (the symbol $'$ stands for the conjugated transpose, that is $v' \equiv \tilde{v}^{\mathsf{T}}$) is a fourth degree polynomial in κ_m, namely

$$F(\kappa_m; u_m) = \mathbf{r}'\mathbf{r} = c_0 + c_1 \kappa_m + c_2 \kappa_m^2 + c_3 \kappa_m^3 + c_4 \kappa_m^4, \tag{19}$$

where

$$c_0 = \mathbf{a}_0'\mathbf{a}_0, c_1 = \mathbf{a}_0'\mathbf{a}_1 + \mathbf{a}_1'\mathbf{a}_0, c_2 = \mathbf{a}_0'\mathbf{a}_2 + \mathbf{a}_2'\mathbf{a}_0 + \mathbf{a}_1'\mathbf{a}_1, c_3 = \mathbf{a}_1'\mathbf{a}_2 + \mathbf{a}_2'\mathbf{a}_1 \text{ and } c_4 = \mathbf{a}_2'\mathbf{a}_2.$$

Thus, for a given value of $\mathbf{u}_m$, the wave number κ_m minimizing the squared residual $F(\kappa_m; u_m)$ is explicitly found by solving the cubic equation

$$\frac{dF}{d\kappa_m} = c_1 + 2c_2 \kappa_m + 3c_3 \kappa_m^2 + 4c_4 \kappa_m^3 = 0. \tag{20}$$

Note that despite the fact that vectors $\mathbf{a}_i$, for $i = 0, 1, 2$ are complex, coefficients c_i, for $i = 0, 1, 2, 3, 4$, are real and there is at least one real root of (20). In the case the three roots are real, two of the roots are associated with local minima because F is a nonnegative function. The root selected is the one providing the absolute minimum provided it is not negative: in all the examples it coincides with the root closer to the exact value κ.

In the next section, this idea is used to assess the numerical wave number κ_H associated with the numerical solution u_H. This is performed selecting $\mathbf{u}_m$ properly representing the solution u_H

4.2 A new paradigm in a posteriori error assessment: best fitting of the modified equation

As previously announced, the goal of this section is to select $u_m \approx u_H$, and then define κ_H as the parameter of the modified problem that better accommodates u_m, namely

$$\kappa_H := \underset{\kappa_m}{\operatorname{argmin}} F(\kappa_m; u_m). \tag{21}$$

Note that the function u_m is in fact described by the vector of nodal values $\mathbf{u}_m$ representing it in the reference h-mesh.

Thus, an a posteriori error estimate for the wave number can be readily computed

$$E = \kappa - \kappa_H. \tag{22}$$

The question is now how to select a proper $\mathbf{u}_m$ approximating u_H.

The idea is to imitate the derivation of the a priori estimate described in section 3. Recall that κ_H was selected as the value of κ_m such that u_m was coinciding with u_H at the nodes P_j, $j = 1, 2, \ldots, n_H$, of the H-mesh. In the 1D model problem selected in section 3, the solution u_m is explicitly found as a function of κ_m and therefore κ_H (in its a priori version, κ_H^{pri}) is readily obtained.

A similar procedure is proposed here in the context of the discrete modified problem (17) defined in the h-mesh. Now, for a given value of κ_m, the solution u_m of the modified problem is subjected to an additional constraint imposing that u_m coincides with u_H at the nodes of the coarse H-mesh, that is at P_j, $j = 1, 2, \ldots, n_H$.

That is, for a given value of κ_m, the constrained modified problem reads

$$\begin{aligned} &[\mathbf{K}_h + i\rho c A_n \kappa_m \, \mathbf{C}_h - \kappa_m^2 \mathbf{M}_h] \, \mathbf{u}_m = -i\rho c \kappa_m \, \mathbf{f}_h \\ &\text{enforcing the additional constraint } \; u_m|_{P_j} = u_H|_{P_j} \end{aligned} \tag{23}$$

The additional constraints are simply enforced using the Lagrange multipliers technique. The resulting solution u_m is expressed in the h-mesh. The residual $\mathbf{r}$ associated with the solution u_m is defined as in (18) and it depends explicitly on u_m through the coefficients c_j, $j = 0, \ldots, 4$, and the vectors $\mathbf{a}_j$, $j = 0, 1, 2$. Note that $\mathbf{r}$ is not null because the additional constraints induce unbalanced reaction terms.

Thus, function F is defined and computed exactly as in (19). The only difference is that now u_m is not given a priori but is a function of κ_m obtained by solving (23). Thus, F depends only on κ_m but in a more complex way and, consequently, F is not anymore a polynomial in κ_m. The numerical wave number κ_H is defined to be the value of κ_m minimizing F. This value results from solving an optimization problem and the minimum is attained for the value κ_H corresponding to the solution of (23) denoted as $\mathbf{u}_m^{\text{opt}}$. Once κ_H is available, the corresponding estimate is readily computed: $E = \kappa - \kappa_H$.

Note that for a given $\mathbf{u}_m^{\text{opt}}$, ignoring the value of κ_m, one could compute the corresponding vectors and coefficients and derive the value of κ_m solving the cubic equation (20). The result of this procedure is denoted as κ_H^{min} and the corresponding error estimate is $E^{\text{min}} = \kappa - \kappa_H^{\text{min}}$.

The computation of $\mathbf{u}_m^{\text{opt}}$ and κ_H is computationally unaffordable in a practical application. The optimization problem requires solving many times problem (23), which in every occasion results in a large system of equations in the reference mesh. Consequently this can only be performed for academic examples. On the other hand, once $\mathbf{u}_m^{\text{opt}}$ is obtained, the computation of κ_H^{min} is explicit and does not require solving any system of equations.

It is observed in all the test cases that the values of κ_H and κ_H^{min} are practically identical. That is, once the function $\mathbf{u}_m^{\text{opt}}$ is found, the corresponding wave number is exactly computed solving explicitly the cubic equation (20).

In any case, both κ_H and κ_H^{min} behave well in the sense that they match the a priori estimates described in section 3 and the measured values of κ_H in the cases where such a measure is feasible.

Following this idea, the dispersion error is isolated of interpolation error because the shape of the modified solution in the interior of the elements of the coarse H-mesh is recovered as the solution of the constrained modified equation (23).

Remark 1 *In order to obtain a computable estimate, the definition of κ_H introduced above depends on the selected reference mesh of characteristic size h. For the sake if simplicity, the dependence of κ_H with h is omitted in the notation. A notation explicitly stating the dependence of h, for instance $\kappa_{H;h}$, would be more accurate. The definition is however consistent in the sense that for h tending to zero, the limit value $\kappa_{H;0}$ is actually the solution of a continuous problem that can be stated as follows.*

The continuous counterpart of (23)*, that is the constrained modified equation, reads: find $u_m \in \mathcal{H}^1(\Omega)$ such that $u_m = u_H$ at the nodes of the H-mesh (that is $u_m|_{P_j} = u_H|_{P_j}$ for $j = 1, 2, \ldots, n_H$) and fulfilling*

$$a_m(\kappa_m; u_m, v) = l_m(\kappa_m; v)$$

for all $v \in \mathcal{H}^1(\Omega)$ *such that* $v|_{P_j} = 0$ *for* $j = 1, 2, \ldots, n_H$*, where*

$$a_m(\kappa_m; u, v) := \int_\Omega \nabla u \cdot \nabla \tilde{v}\, d\Omega - \int_\Omega \kappa_m^2 u \tilde{v}\, d\Omega + \int_{\Gamma_R} i\rho c \kappa_m A_n u \tilde{v}\, d\Gamma$$
$$\text{and } l_m(\kappa_m; v) := -\int_{\Gamma_N} i\rho c \kappa_m \bar{v}_n \tilde{v}\, d\Gamma.$$

Thus, κ_H *is selected as the value of* κ_m *minimizing the residual of the non-constrained problem. Let us introduce the residual as*

$$R(\kappa_m; u_m; v) := l_m(\kappa_m; v) - a_m(\kappa_m; u_m, v)$$

for any v *in* $\mathcal{H}^1(\Omega)$*. Note that the value of* $R(\kappa_m; u_m; v)$ *is only equal to zero if* $v|_{P_j} = 0$ *for* $j = 1, 2, \ldots, n_H$*). For* v *functions taking non-zero values at nodes, the residual is not null. The scalar measure of the residual* $R(\cdot)$ *is introduced as*

$$F(\kappa_m; u_m) := \max_{v \in \mathcal{H}^1(\Omega) \setminus \{0\}} \frac{R(\kappa_m; u_m; v)}{\|v\|}$$

Thus, the value of κ_H *is retrieved as the value of* κ_m *minimizing* F*, as indicated in equation* (21) *(the expression is valid both for the reference* h*-solution and the continuous case).*

Note that in the case that it exists a value of κ_m *such that the solution of the non-constrained problem coincides with* u_H *at the nodes* P_j*, this value of* κ_m *is precisely* κ_H *because for this value and the corresponding* u_m*,* F *vanishes.*

The definition of a practical error estimate following this rationale requires introducing a proper approximation to $\mathbf{u}_m^{\text{opt}}$, resulting from a computationally affordable procedure.

4.3 Interpolation of u_H *in the* h*-mesh*

The first and obvious choice is to set u_m as the interpolant of u_H in the h-mesh, $[u_H]_h$. Since in practice the finer h-mesh is nested in the coarser H-mesh, $[u_H]_h$ is an exact representation of u_H.

For this choice the vector of nodal values $\mathbf{u}_m$ is readily obtained: at the nodes of the coarse mesh P_i, for $i = 1, 2, \ldots, n_H$, u_m and u_H coincide. At the rest of the nodes of the h-mesh, the nodal value is obtained by simple interpolation in the element of the coarse H-mesh where the node is located.

Once $\mathbf{u}_m$ is computed the corresponding value of κ_H^{int} is calculated analytically solving the cubic equation (20). Recall that the coefficients c_1, c_2, c_3 and c_4 depend

on the choice for $\mathbf{u}_m$. As previously said, in the case the three roots are real the one selected is the absolute minimum of F which in all the test cases coincides with the closest root to κ. Once the value of the numerical wave number κ_H^{int} is assessed, the corresponding error estimate follows:

$$E^{\text{int}} = \kappa - \kappa_H^{\text{int}}. \tag{24}$$

As it is shown in the examples presented in section 6, the approximations to κ_H provided with this methodology are not as good as expected when compared with the measured numerical wave number (this measurement can be performed in very simple test examples) or with the a priori estimates. The estimates obtained using this strategy are not as sharp as desired, with effectivity indices between 70% and 90% in the simpler example. However, with the methods proposed below, the effectivity index from 86% to 100%.

This behavior is explained using the following rationale: the interpolated function $[u_H]_h$ is not a *natural* solution of a modified equation (17). The function $[u_H]_h$ is piecewise linear in the elements of the coarse H-mesh and no solution of (17) would fulfill this type of constraint. A typical solution of (17) is smoother, without the slope discontinuities concentrated in the nodes P_i, for $i = 1, 2, \ldots, n_H$, of the coarse H-mesh. In other words, we cannot expect to find a value of κ_m properly accommodating $[u_H]_h$ in (17).

Moreover, in the a priori analysis sketched in section 3 only the nodal values of the numerical solution are used to recover the numerical wave number κ_H. No information about the value of u_H inside the elements enters the analysis. This makes complete sense because only the dispersion/pollution part of the error is to be assessed. Including the information inside the elements would result in assessing also the interpolation error.

Consequently, in the value of κ_H^{int} assessed with the a posteriori strategy described here (using $u_m = [u_H]_h$), the effects of both the dispersion error (error in κ) and the interpolation error are taken into account together. Next section is devoted to introducing a new strategy allowing to assess the dispersion error separately.

4.4 Enhanced solution $u^\star$ by postprocessing of u_H

The methodology introduced in section 4.2 is not applicable as a practical error estimation strategy. The error estimation procedure cannot be based on solving problems in the complete finer reference mesh. It has been noted also that once the function $\mathbf{u}_m^{\text{opt}}$ is found, the corresponding wave number is fairly computed solving explicitly the cubic equation (20). The idea proposed here is to build up an inexpensive approximation of $\mathbf{u}_m^{\text{opt}}$ using a postprocessing technique standard in error

estimation analysis [19,8] and likely having all its features. This approximation is expressed as a nodal vector in the finer h-mesh and it is denoted by $\mathbf{u}^\star$. Once $\mathbf{u}^\star$ is obtained from $\mathbf{u}_H$, the corresponding wave number $\kappa_H^\star$ is readily computed solving the cubic equation (20) and hence $E^\star = \kappa - \kappa_H^\star$.

The enhanced solution is produced locally, in patches of elements, centered in every element of the mesh. The values of $\mathbf{u}_H$ at the nodes of the H-mesh are used as the input data and a polynomial is fitted using a least squares technique. The degree of the polynomial fitted is larger than the degree of the finite elements used to compute u_H. For every element Ω_n, $n = 1, \ldots, n_{\mathsf{el}}$, of the H-mesh, the patch of elements surrounding Ω_n is considered. The polynomial fitting the values of u_H in the nodes of the patch is computed. Once the polynomial is obtained it is evaluated to find the nodal values of $u^\star$ in the nodes of the h-mesh lying in element Ω_n of the H-mesh. This is illustrated in figure 4. This approach allows to recover the natural curvatures of the solution coinciding with u_H at the nodes where it is computed. Reference [6] describes the details of the least squares fitting strategy.

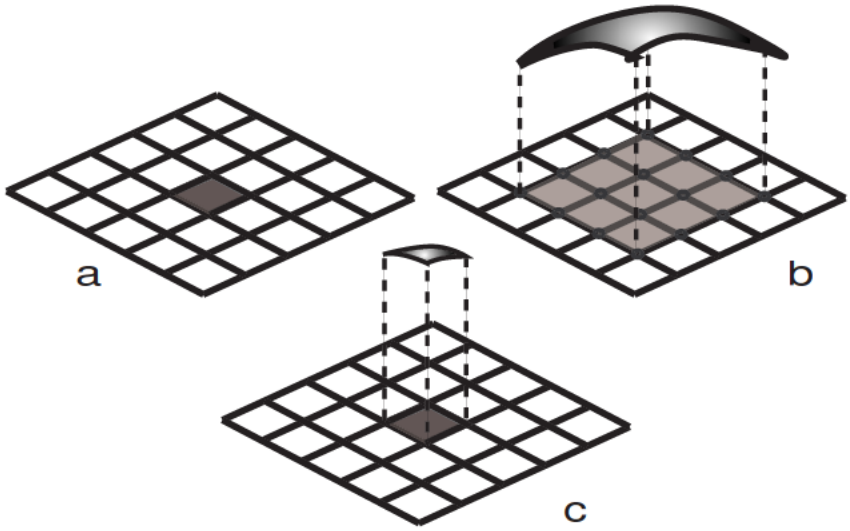

Fig. 4. Every element of the H-mesh (darkened in plot a) is associated with a patch (shadowed in plot b). A polynomial is fitted to the values in the nodes in this patch using a least squares criterion (b). This polynomial is evaluated to obtain the nodal values of the enhanced function $u^\star$ in the nodes of the refined h-mesh in the element under consideration (c).

As it is shown in the numerical tests, this strategy provides a fair and inexpensive approximation $\mathbf{u}^\star$ of the optimal solution $\mathbf{u}_m^{\mathrm{opt}}$ of the constrained modified problem (23), which is computationally unaffordable. The corresponding numerical wave number assessment and error estimate, $\kappa_H^\star$ and $E^\star$, perform well, similarly as the computationally unaffordable estimates κ_H and κ_H^{min}.

The reference mesh in which $\mathbf{u}^\star$ is supported is described above as generated by h-refinement. Obviously, the p-refined analogous strategy is readily defined by just using a higher order H-mesh and by using the locally fitted polynomial to compute

the nodal values of $u^\star$ in the p-refined discretization. As it is shown in the examples, the results produced by the p-refined solution are not as good. This is probably due to the loss of accuracy observed in parts of the frequency spectrum when using standard p-refinement, as suggested by Hughes [7,10].

4.5 Correction factor introduced to account for the finite size h of the reference mesh

The estimates introduced in the previous section rely on a reference discretization of mesh size h which supposedly provides a more accurate solution than the computed H-approximation. In practice, h is far from being infinitesimal and it is taken as a subdivision of H, namely $h = H/n_r$ with relatively small values of n_r (in the examples $n_r = 2$) in order to lower the computational cost of the estimate.

Thus, in practice, the values of the assessed error are with respect to the numerical wave number corresponding to the h-mesh, κ_h. The different values of E obtained in the previous sections are approximations to $\kappa_h - \kappa_H$ and not to $\kappa - \kappa_H$ as it could be expected.

Here, a correction factor is introduced to account for this fact, based on a Richardson-like extrapolation strategy [16].

The a priori estimate (16), described in section 3, is assumed to hold for both the H-mesh and the h-mesh, that is

$$\kappa - \kappa_h \approx \frac{\kappa^3 h^2}{24} \text{ and } \kappa - \kappa_H \approx \frac{\kappa^3 H^2}{24}$$

It follows that

$$\kappa_h - \kappa_H = \frac{\kappa^3}{24}(H^2 - h^2)$$

and using $h = H/n_r$ yields

$$\kappa_h - \kappa_H = \frac{\kappa^3 H^2}{24}\left(1 - \frac{1}{n_r^2}\right)$$

That is

$$\kappa - \kappa_H = \frac{n_r^2}{(n_r^2 - 1)}(\kappa_h - \kappa_H) \tag{25}$$

Thus, the factor $n_r^2/(n_r^2 - 1)$ (4/3 for $n_r = 2$) is used to correct the estimates which are, in principle, assessing the error with respect to κ_h. Using above correction, we are now able to estimate the error with respect to κ.

5 Local version

As previously said, once the recovered function $\mathbf{u}^\star$ is obtained, the estimate $E^\star$ is easily computed. Moreover, a local version of the estimator giving local values of the wave number and, hence, of the error is also straightforward. The goal is to approximate the value of the numerical wave number associated with the element Ω_n, $n = 1, \ldots, n_{\mathsf{el}}$, of the H-mesh. Let us denote this value by κ_H^n. The idea is simply to minimize the local version of the squared residual (19) corresponding to a patch of elements around Ω_n. This approach is simple to implement and computationally inexpensive.

In order to obtain enough information and to properly recover κ_H^n, the patch of elements around Ω_n must be of size larger than a wavelength. This often requires using patches of more than one layer of elements around Ω_n. Figure 5 illustrates both, the simplest case of a patch including just the first layer of elements around Ω_n and a second patch including two layers of elements, corresponding to a larger wave number.

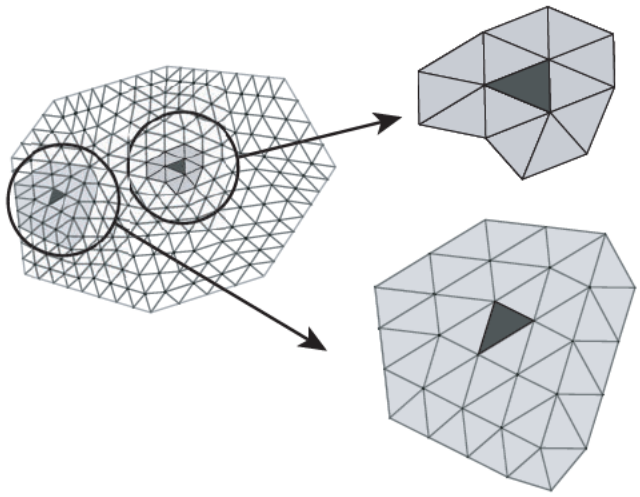

Fig. 5. Every element of the mesh (darkened) generates a patch of all the elements in contact with it (shadowed in gray). Two different patches are shown corresponding to required sizes associated with different wavelengths.

Thus, the local version of the residual corresponding to patch n is

$$\mathbf{r}^n(\kappa^n) = \mathbf{a}_0^n + \mathbf{a}_1^n \kappa^n + \mathbf{a}_2^n (\kappa^n)^2, \tag{26}$$

where $\mathbf{r}^n$ is a function of κ^n and $\mathbf{a}_0^n$, $\mathbf{a}_1^n$ and $\mathbf{a}_2^n$ are defined as in section 4, using $\mathbf{u}^\star$ as the modified function.

Then, the approximation for the local wave number κ_H^n is determined minimizing the squared local residual:

$$\kappa_H^n := \underset{\kappa^n}{\operatorname{argmin}} (\mathbf{r}^{n\prime} \mathbf{r}^n). \tag{27}$$

Recall that solving this minimization problem is a purely explicit calculation because it only requires finding the roots of (20).

6 Numerical examples

The strategy to assess the error in the wave number presented in the previous sections is validated in three numerical examples.

6.1 Example 1: 1D strip

The first example is a 1D problem solved in a rectangular domain as illustrated in Fig. 6. This simple case allows testing the performance of the estimates provided by comparing them with the actual values that, in this case, can be easily measured.

Equation (3) is solved in the rectangular domain shown in figure 6, with $\rho c = 1$, $A_n = -1$ and $\kappa = 8\pi$ (such that the wavelength is 1/4 and therefore the solution has four complete waves in the domain of length L=1).

Dirichlet boundary condition is imposed on the left side of the boundary, equation (5) with $\bar{u} = 1$, while Robin boundary condition (denoted also as ficticious boundary condition) is enforced on the right lateral side. The boundary condition on the upper and lower horizontal boundaries are assumed to be Neumann homogeneous to keep the 1D character of the solution.

The solution $u(x, y)$ of the problem is independent of y and its analytical expression is

$$u(x, y) = \cos(\kappa x) + i \sin(\kappa x)$$

This solution obviously fulfills (3), with Dirichlet boundary conditions (5) and Robin boundary conditions (7), respectively

$$u(0, y) = 1 \quad \text{at} \quad x = 0$$

$$\frac{\partial u}{\partial x}(1, y) = i\kappa u(1) \quad \text{at} \quad x = 1$$

Having at hand the analytical expression for $u(x, y)$ allows computing a direct measure of the error in the wave number or, conversely, in the wavelength. Let u_H^L be the average value of the real part of the numerical solution at $x = L$ (for uniform quadrilateral meshes all the nodal values are equal on this line). Then the error in wavelength is denoted by $\Delta\lambda$ and satisfies

$$u(x = L - \Delta\lambda) = u_H^L \tag{28}$$

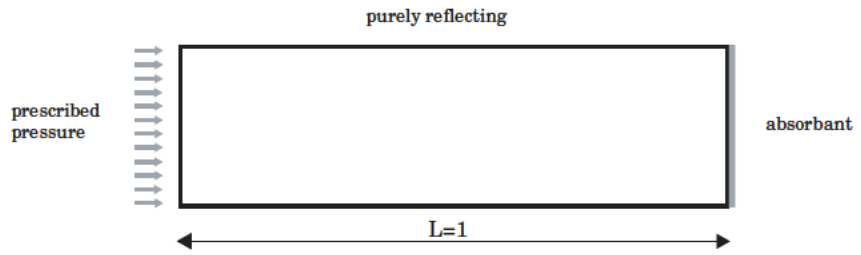

Fig. 6. Example 1; 1D strip: problem setup.

taking the real part of above equation, we obtain

$$\cos(\kappa(L-\Delta\lambda)) = \mathrm{Re}(u_H^L) \Rightarrow \Delta\lambda = -\frac{\arccos(u_H^L)}{\kappa} + L \tag{29}$$

The wavelength error $\Delta\lambda$ is equally distributed among the n periods present in the domain, where $n = L/\lambda$ and $\lambda = 2\pi/\kappa$. Thus the measure of numerical wavelength is $\lambda_H = \lambda + \Delta\lambda/n$ and, consequently

$$\kappa_H^{\text{meas}} = \frac{2\pi}{\lambda_H} \tag{30}$$

Thus, the resulting a posteriori measure of the dispersion is

$$E^{\text{meas}} = \kappa - \frac{2\pi}{\left(\lambda + \frac{\Delta\lambda}{n}\right)} \tag{31}$$

where $\Delta\lambda$ is given by (29).

The problem is numerically approximated using quadrilateral meshes (4-nodel bilinear elements), starting from a coarse mesh of 24×2 elements (in the x-direction $H = 1/24$, i.e 6 elements per wavelength. The corresponding approximation is depicted in figure 7).

The error estimates described in the previous sections are computed using a refinement factor $n_r = 2$ in order to reduce the computational cost.

The numerical results are summarized in Tables 1, 2 and 3. Each row in the tables corresponds to a different mesh. Due to the 1D character of the problem the meshes are only refined in the x-direction. The consecutive meshes have two rows of elements. The size of the element in the x-direction is therefore $H = 2/n_{el}$. The different value for κ_H are displayed in Table 1, that is $\kappa_H^{\text{pri}}, \kappa_H^{\text{meas}}, \kappa_H^{\text{int}}, \ldots, \kappa_H^{\star}$ corresponding to the notation introduced above. Table 2 shows the corresponding error estimates and the effectivity indices with respect to the measured value, namely

$$\theta^{\square} = \frac{E^{\square}}{E^{\text{meas}}} \tag{32}$$

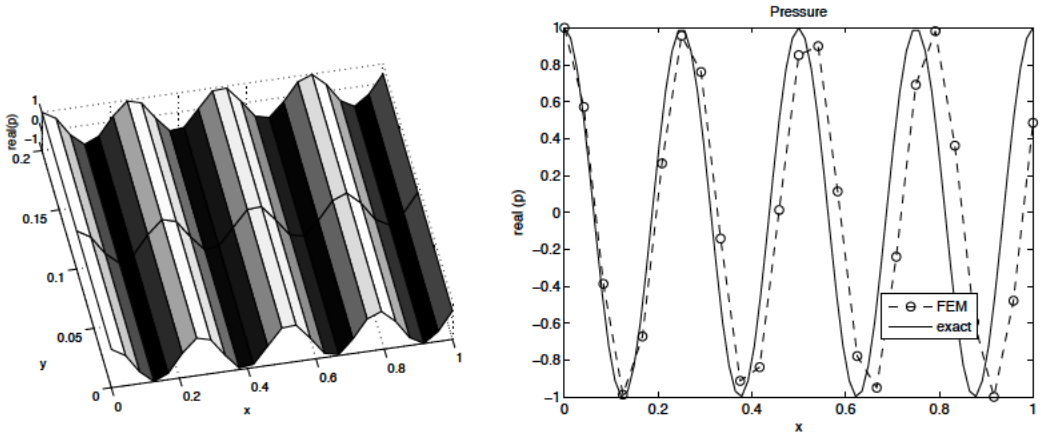

(a) (b)

Fig. 7. *Distribution pressure (a) and dispersion effect (b) for wave number* $\kappa = 8\pi$ *in a structured quadrilateral mesh.*

Table 3 is analogous to table 2 but for a p-refined reference discretization, where the correction factor introduced in the section 4.5 cannot be applied.

dof	n_{el}	H	κ_H^{pri}	κ_H^{meas}	κ_H^{int}	κ_H	κ_H^{min}	$\kappa_H^{\star}$
75	48	1/24	23.9844	24.1126	24.4287	24.3595	24.3622	24.3643
99	64	1/32	24.4868	24.5196	24.6672	24.6795	24.6788	24.6989
123	80	1/40	24.7193	24.7315	24.7980	24.8295	24.8346	24.8610
147	96	1/48	24.8456	24.8513	24.8773	24.9195	24.9233	24.9497

Table 1
Example1: Degrees of freedom dof; number elements n_{el}; interval of mesh H and wave numbers κ_H.

dof	E^{pri}	E^{meas}	E^{int}	θ^{int}	E	θ	E^{min}	θ^{min}	$E^{\star}$	$\theta^{\star h}$
75	4.569	4.059	3.734	0.92	4.102	1.01	4.089	1.00	4.077	1.0044
99	2.570	2.439	2.469	1.01	2.405	0.98	2.408	0.98	2.301	0.9434
123	1.644	1.596	1.774	1.11	1.609	1.08	1.582	0.99	1.442	0.9033
147	1.142	1.119	1.354	1.21	1.131	1.01	1.111	0.99	0.971	0.8671

Table 2
Example1: Values of the relative dispersion error (%) a priori, measured and for the case h-refined solution with the respective effectivity indices.

The analysis of the results of tables 1, 2 and 3 reveals that the estimate E and E^{min} are yielding very good approximations of the actual error E^{meas}. Recall however that these two quantities are not computationally affordable in a practical context and have been produced only as an academic illustration of the presented paradigm. The two practical estimates E^{int} and $E^{\star}$ are also showing a good behavior, especially if the reference mesh is build up using h-refinement (table 2). When using

dof	κ_H	E	θ	$\kappa_H^{\min}$	$E^{\min}$	$\theta^{\min}$	$\kappa_H^\star$	$E^\star$	$\theta^\star$
75	24.0995	4.111	1.01	24.1088	4.074	1.00	23.4682	6.623	1.63
99	24.5295	2.400	0.98	24.5311	2.394	0.98	24.1255	4.007	1.64
123	24.7295	1.605	1.00	24.7324	1.593	0.99	24.4709	2.633	1.65
147	24.8495	1.127	1.00	24.8514	1.119	0.99	24.6703	1.839	1.64

Table 3
Example1: Values of wave numbers and relative dispersion error (%) correspondent to solution p-refined and the respective effectivity indices.

p-refinement (table 3), the effectivity is degraded probably due to the effect suggested at the end of section 4.4. It is worth noting that the estimate $E^\star$ is, as expected, sharper than E^{int}.

The convergence of the dispersion error when reducing H is shown in figure 8. Note that the horizontal axis in these plots corresponds to $\log dof$ which is equal to $-\log H$ up to an additive constant. The plot on the top describes the convergence behavior for the estimates taking as a reference solution an h-refined one. The second plot is the analogous with a p-refined reference solution. The results demonstrate that all the proposed estimates converge at the due rate, compared with the a priori and the measured dispersion errors. Moreover, the h-refined reference mesh estimates yields sharper results than the p-refined ones in all the tests.

Finally, the spatial error distribution corresponding to the local (elementary) contributions to the dispersion error as described in section 5 is displayed in figure 9. The second plot corresponds to a variant of the problem where the Dirichlet boundary conditions at the left side are replaced by Neumann type boundary condition. It is worth noting that the local contributions to the dispersion error are, as expected, sensitive to the selected boundary conditions.

6.2 Example 2: 2D acoustic problem in L-Shaped domain

The second example has a full 2D character. The L-shaped domain shown in figure 10 is considered. The size of the domain is set by the values $L_1 = 0.8$ m and $L_2 = 0.2$ m. Most of the domain boundary is of Neumann type, homogeneous everywhere on the boundary except on the top left edge where the velocity is prescribed to be $\bar{v}_n = 1$ m/s (this corresponds to a vibrating panel, see Figure 10). Moreover, the bottom side is an absorbent material, corresponding to a Robin boundary condition 7 with $A_n = 1/\rho c$ m/Pa.s.

The wave number is $\kappa = 8\pi$, as in the previous example. The solution computed with a coarse mesh is displayed in figure 11.

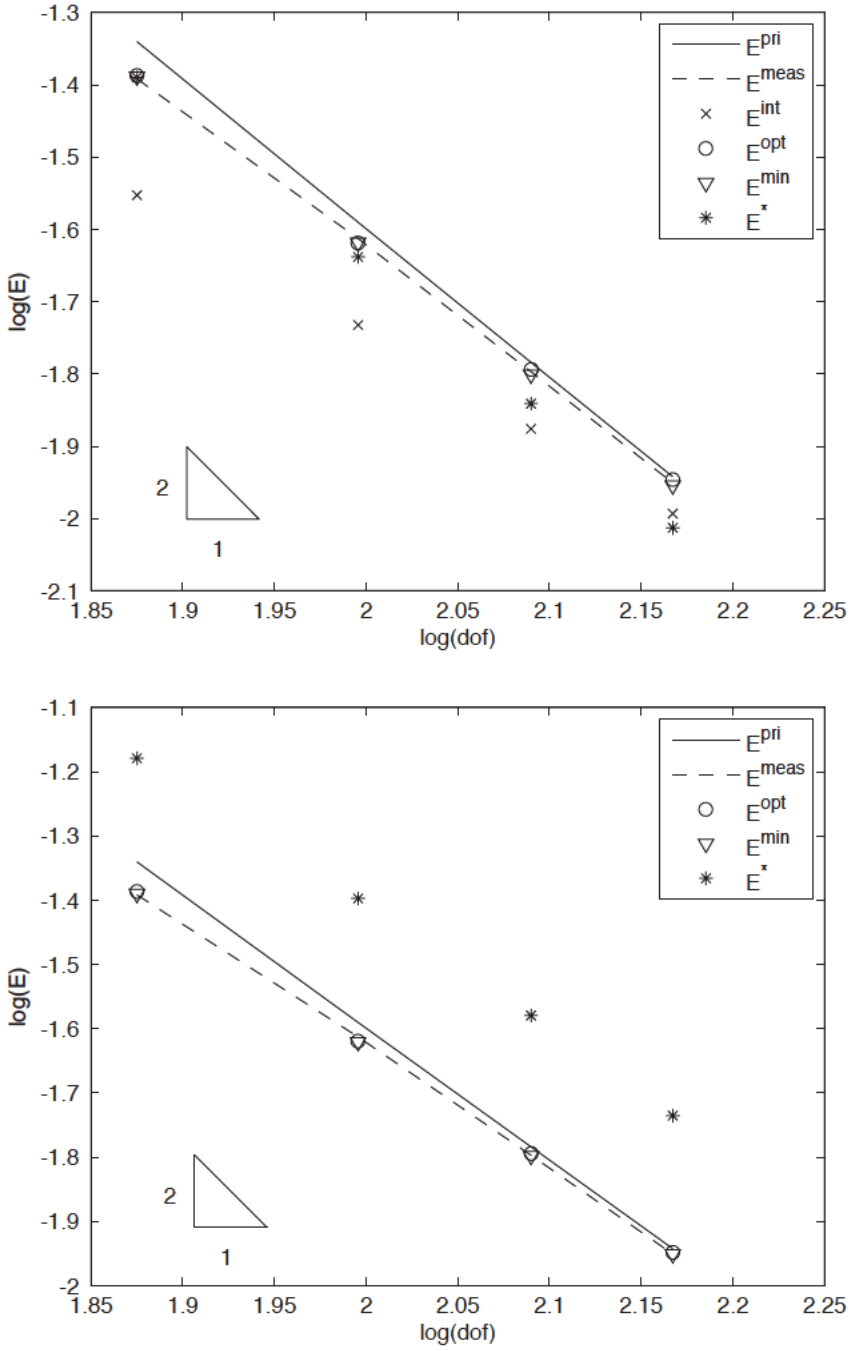

Fig. 8. *Example 1: Convergence of the error for the h-refined reference mesh (top) and the p-refined reference mesh (bottom).*

The estimates E, E^{min} and $E^{\star}$ are computed for three series of refined meshes; structured quadrilaterals, structured triangles and unstructured triangles. The results are displayed in tables 4, 5 and 6, respectively. The practical error estimate $E^{\star}$ produces values that are reasonable approximations of the more accurate but computationally unaffordable estimates E and E^{min}.

The convergence of the different series of refined meshes is shown in figure 12.

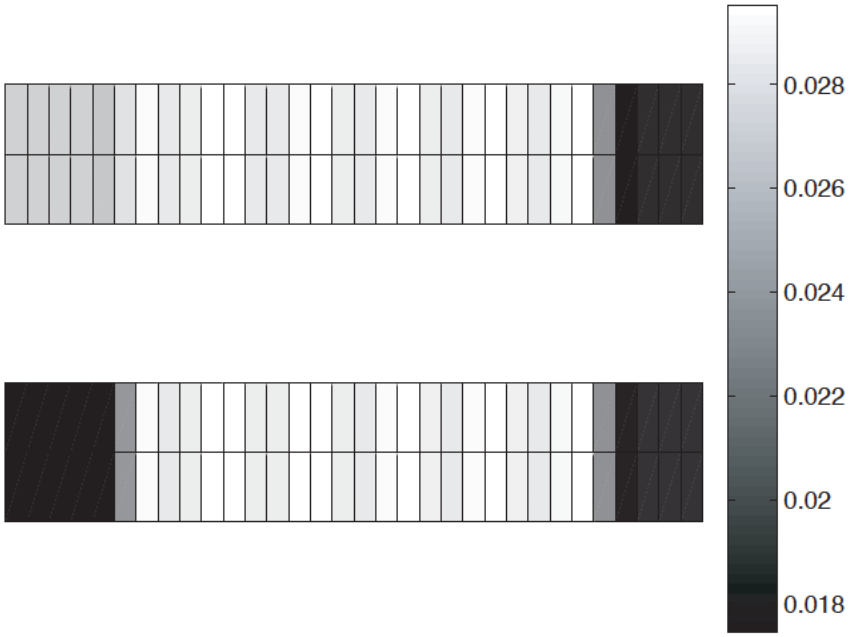

Fig. 9. Example 1: Spatial error distribution of the error for the problem for stated in figure 6 (top) and for a variant with Neumann boundary condition of the left side (bottom).

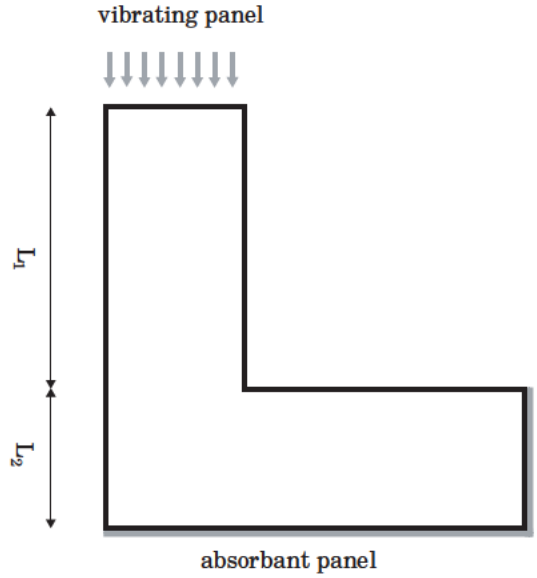

Fig. 10. Example 2: 2D L-Shaped domain and boundary conditions.

Note that in this 2D case the relation between the number of degrees of freedom (dof) and H is different, dof is proportional to $1/H^2$, i.e. $\log dof$ is equal to $-2\log H$ up to an additive constant.

One can observe in the plots of figure 12 that the estimate $E^\star$ is behaving similarly to the reference estimates E and E^{min}.

The slope of the curves given by E and E^{min} is (approximately) equal to 1 as pre-

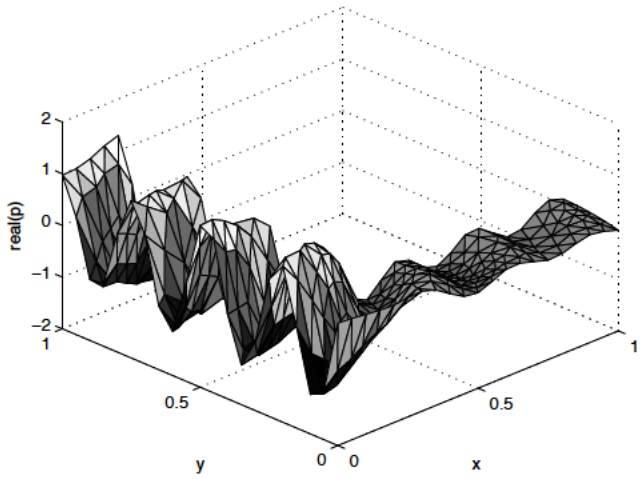

Fig. 11. Example 2: Real part of the acoustic pressure computed with an unstructured triangular mesh of 281 dof and 480 elements.

dof	n_{el}	κ_H	E	$\kappa_H^{\min}$	$E^{\min}$	$\kappa_H^\star$	$E^\star$
57	36	22.9895	8.528	21.8287	13.146	22.7910	9.317
185	144	24.0795	4.191	24.1039	4.093	24.1424	3.940
657	576	24.8395	1.167	24.8507	1.122	24.9077	0.895

Table 4
Example 2: Results corresponding to structured quadrilateral meshes.

dof	n_{el}	κ_H	E	$\kappa_H^{\min}$	$E^{\min}$	$\kappa_H^\star$	$E^\star$
57	72	22.6195	10.000	22.5721	10.189	23.9924	4.537
185	288	24.1895	3.753	24.2237	3.617	24.3199	3.234
657	1152	24.8495	1.127	24.8734	1.032	24.9306	0.804

Table 5
Example 2: Results corresponding to structured triangular meshes.

dof	n_{el}	κ_H	E	$\kappa_H^{\min}$	$E^{\min}$	$\kappa_H^\star$	$E^\star$
81	120	22.6195	10.000	22.7151	9.619	23.6310	5.975
281	480	24.3095	3.276	24.3470	3.126	24.5641	2.262
1041	1920	24.9095	0.889	24.9193	0.849	25.0092	0.492

Table 6
Example 2: Results corresponding to unstructured triangular meshes.

dicted by the a priori estimate and the slopes associated with $E^\star$ are 0.96, 0.71 (discrepancy due to a bad result in the first coarse approximation in the series of structured triangular meshes) and 0.98 for the different mesh typologies. The figure 13 shows the spatial error distribution for the second mesh of each of the refinement series (meshes with 144 structured quadrilaterals, 288 structured triangles and 480

unstructured triangles).

6.3 Example 3: 2D acoustic car cavity

Noise transmission inside the interior of passenger cars is considered as a practical application. This example has been frequently used as a benchmark in error assessment for interior acoustics [5,18].

The size of the domain is characterized by the maximum horizontal and vertical lengths, $L_x = 2.7$ m and $L_y = 1.1$ m, respectively. The values of the material parameters are $\rho = 1.225$ Kg/m^3 (density) and $c = 340$ m/s (speed of sound). Figure 14 describes the geometry of the domain and the boundary conditions: a unit normal velocity $\bar{v}_n = 1$ m/s is imposed on the left vertical side. The roof is considered to be an absorbant panel with $A_n = 1/2000$ m/Pa.s and the rest of the boundary is assumed to be perfectly reflecting ($\bar{v}_n = 0$).

The wave number of the incoming vibrations $\kappa = 9.7$ corresponds to a frequency of 525 Hz. The figure 15 shows the distribution of the real part of the pressure and the pressure distribution along of the line A displayed in figure 14. The two curves correspond to a coarse and a finer computational meshes. Note that, compared with the finer mesh, the dispersion error in the coarse mesh is important.

The strategy to asses the dispersion error introduced in this paper is used in a series of uniformly refined FE meshes. The results are shown in Table 7 and Figure 16. The estimate $E^\star$ is showing again a good performance, fairly approximating the academic estimates E and $E^{\min}$ and converging at the proper rate (the slope of the line is approximately 1.2). Finally, the error map is displayed in figure 17 and the larger contributions to the error are located at the expected zones.

dof	n_{el}	κ_H	E	$\kappa_H^{\min}$	$E^{\min}$	$\kappa_H^\star$	$E^\star$
137	195	9.0618	6.598	9.0831	6.378	8.5908	11.452
469	780	9.5318	1.754	9.5363	1.708	9.5203	1.872
1718	3120	9.6518	0.517	9.6507	0.529	9.6534	0.501

Table 7
Example 3: Results corresponding to $\kappa = 9.7$, dispersion error in a uniformly refined series of meshes.

An additional numerical experiment is performed for the same problem as described above but for a larger frequency of 1100 Hz, that is a wave number $\kappa = 20.3280$. The results obtained are displayed in table 8. The quality of the estimates is also fair for this larger frequency. A good agreement is observed between the reference value E and the estimates $E^{\min}$ and $E^\star$.

dof	n_{el}	κ_H	E	$\kappa_H^{\min}$	$E^{\min}$	$\kappa_H^\star$	$E^\star$
469	780	18.7052	7.983	18.8382	7.328	18.8105	7.465
1718	3120	19.9152	2.031	19.9200	2.007	19.8178	2.509

Table 8
Example 3: Results corresponding to $\kappa = 20.328$, dispersion error in a uniformly refined series of meshes.

7 Concluding remarks

The strategy introduced is based on the determination of the numerical wave number κ_H as the wave number of a modified problem that better accommodates the numerical solution u_H. The modified problem is defined on a reference refined discretization because the resolution has to be increased to properly describe the oscillatory nature of the solution. Compared to other goal oriented error estimation strategies, the approach proposed here is innovative because it adopts a new paradigm. The computational effort in the error estimation procedure is devoted to obtain the wave number of the approximate solution κ_H instead of the exact one, κ, which is known as a problem data. The error estimator provides reasonable approximations of the actual errors, in agreement also with the measured valued of the dispersion error in the simple cases where they can be evaluated. In the practical cases the results match the expected distributions and converge at the predicted rates.

References

[1] M. Ainsworth and J. T. Oden. *A posteriori error estimation in finite element analysis*. John Wiley & Sons, Chichester, 2000.

[2] I. Babuska, F. Ihlenburg, E. T. Paik, and S. A. Sauter. A generalized finite element method for solving the helmholtz equation in two dimensions with minimal pollution. *Comput. Methods Appl. Mech. Engrg.*, 128:325–359, 1995.

[3] I. Babuska and J. M. Melenk. The partition of unity method. *Internat. J. Numer. Methods Engrg.*, 40:727–758, 1997.

[4] I. Babuska and S. A. Sauter. Is the pollution effect of the fem avoidable for the helmholtz equation considering high wavenumber? *SIAM Review*, 42(3):451–484, 2000.

[5] P. Bouillard and F. Ihlenburg. Error estimation and adaptivity for the finite element method in acoustics: 2d and 3d applications. *Comput. Methods Appl. Mech. Engrg.*, 176(1):147–163, 1999.

[6] G. Calderón and P. Díez. Análisis de diferentes estimadores de error de postproceso para adaptatividad orientada al resultado. *Rev. Int. Mét. Num. Cálc. Dis. Ing.*,

22(2):193–213, 2006.

[7] J. A. Cottrell, A. Reali, Y. Bazilevs, and T. J. R. Hughes. Isogeometric analysis of structural vibrations. *Comput. Methods Appl. Mech. Engrg.*, 195(41-43):5257–5296, 2006.

[8] P. Díez and G. Calderón. Goal-oriented error estimation for transient parabolic problems. *Comput. Mech.*, 39(5):631–646, 2007.

[9] P. Díez, J.J. Egozcue, and A. Huerta. *A posteriori* error estimation for standard finite element analysis. *Computer Methods in Applied Mechanics and Engineering*, 163:141–157, 1998.

[10] T. J. R. Hughes, A. Reali, and G. Sangalli. Duality and unified analysis of discrete approximations in structural dynamics and wave propagation: Comparison of p-method finite elements with k-method nurbs. *Comput. Methods Appl. Mech. Engrg.*, In Press, Corrected Proof, Available online 15 April 2008.

[11] F. Ihlenburg. *Finite Element Analysis of Acoustic Scattering*, volume 132 of *Applied Mathematical Sciences*. Springer-Verlarg, New York, 1998.

[12] F. Ihlenburg and I. Babuska. Dispersion analysis and error estimation of galerkin fininite element methods for the helmoholtz equation. *Int. J. Numer. Methods Engrg.*, 38:3745–3774, 1995a.

[13] F. Ihlenburg and I. Babuska. Finite element solution of the helmholtz equation with high wave number. part 1: The hp-version of the fem. *Comput. Math. Appl.*, 38:9–37, 1995b.

[14] J.T. Oden and S. Prudhomme. Goal-oriented error estimation and adaptivity for the finite element method. *Comput. Math. Appl.*, 41(5-6):735–756, 2001.

[15] N. Parés, P. Díez, and A. Huerta. Subdomain-based flux-free a posteriori error estimators. *Comput. Methods Appl. Mech. Engrg.*, 195(4-6):297–323, 2006.

[16] L. F. Richardson. The approximate arithmetical solution by finite differences of physical problems. *Trans. Roy. Soc. (London)*, A210:307–357, 1910.

[17] J. Sarrate, J. Peraire, and A. T. Patera. A posteriori finite element error bounds for non-linear outputs of the helmholtz equation. *Int. J. Numer. Methods Fluid.*, 31(1):17–36, 1999.

[18] S. Suleau, A. Deraemaeker, and P. Bouillard. Dispersion and pollution of meshless solutions for the helmholtz equation. *Comput. Methods Appl. Mech. Engrg.*, 190:639–657, 2000.

[19] N.-E. Wiberg, L.F. Zeng, and X.D. Li. Error estimation and adaptivity in elastodynamics. *Computer Methods in Applied Mechanics and Engineering*, 101:369–395, 1992.

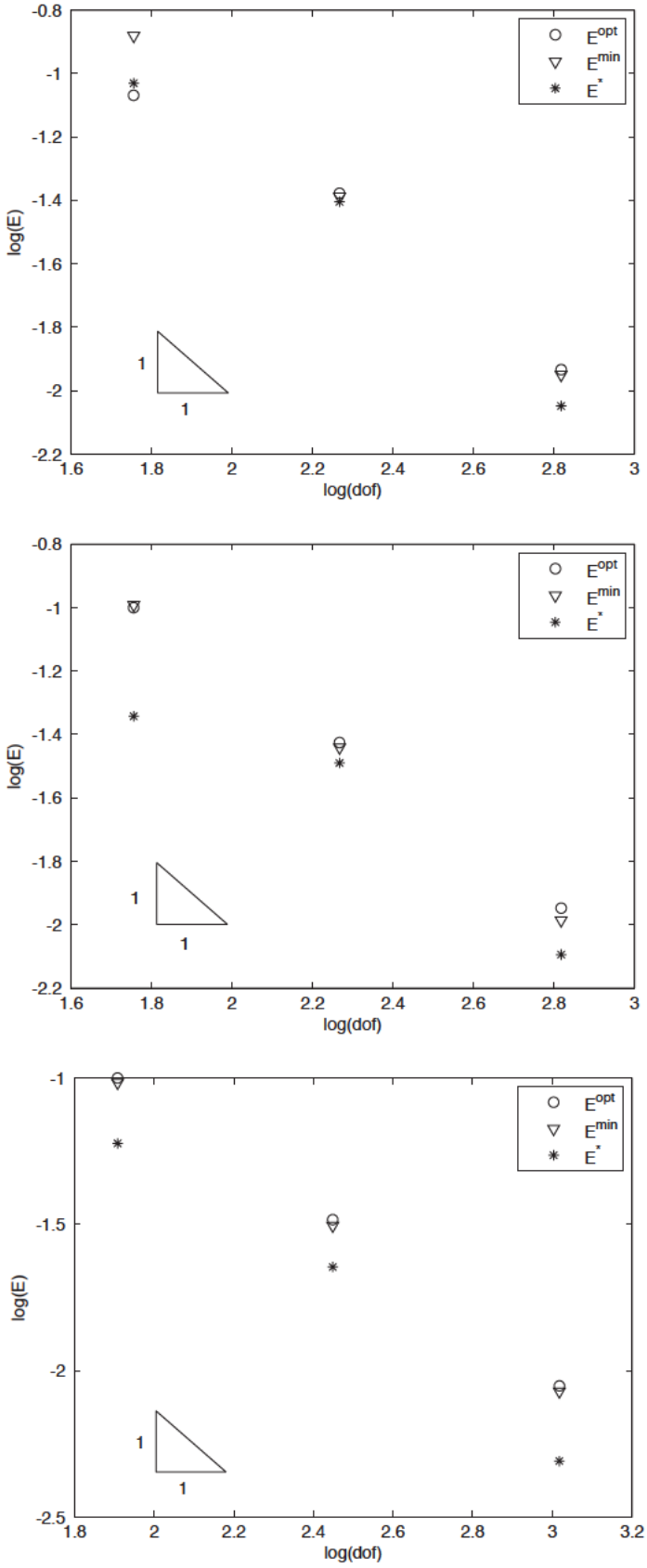

Fig. 12. *Example 2: Convergence of the error in the structured quadrilateral (top), structured triangular (center) and unstructured triangular (bottom) series of meshes.*

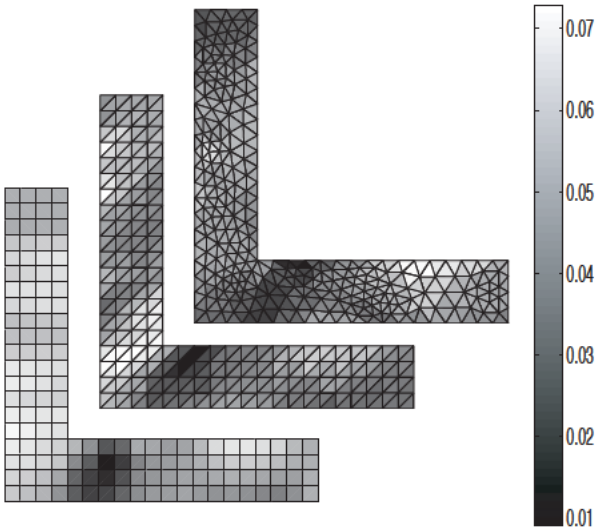

Fig. 13. Example 2: Spatial error distribution for the problem defined in figure 10 in structured quadrilateral and triangular and unstructured triangular meshes.

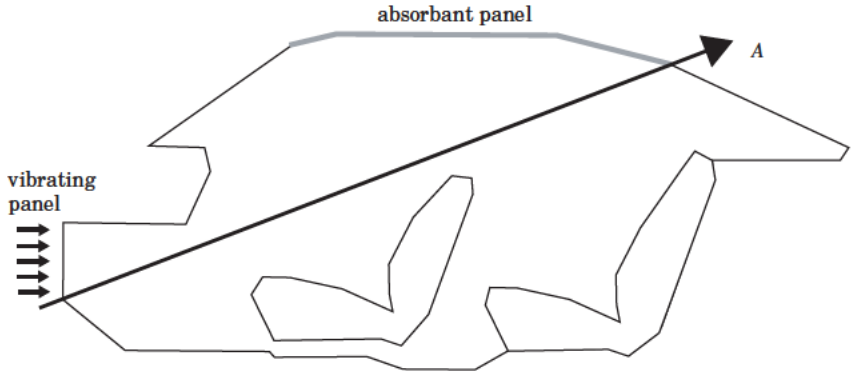

Fig. 14. Example 3: Description of boundary conditions for the car cavity.

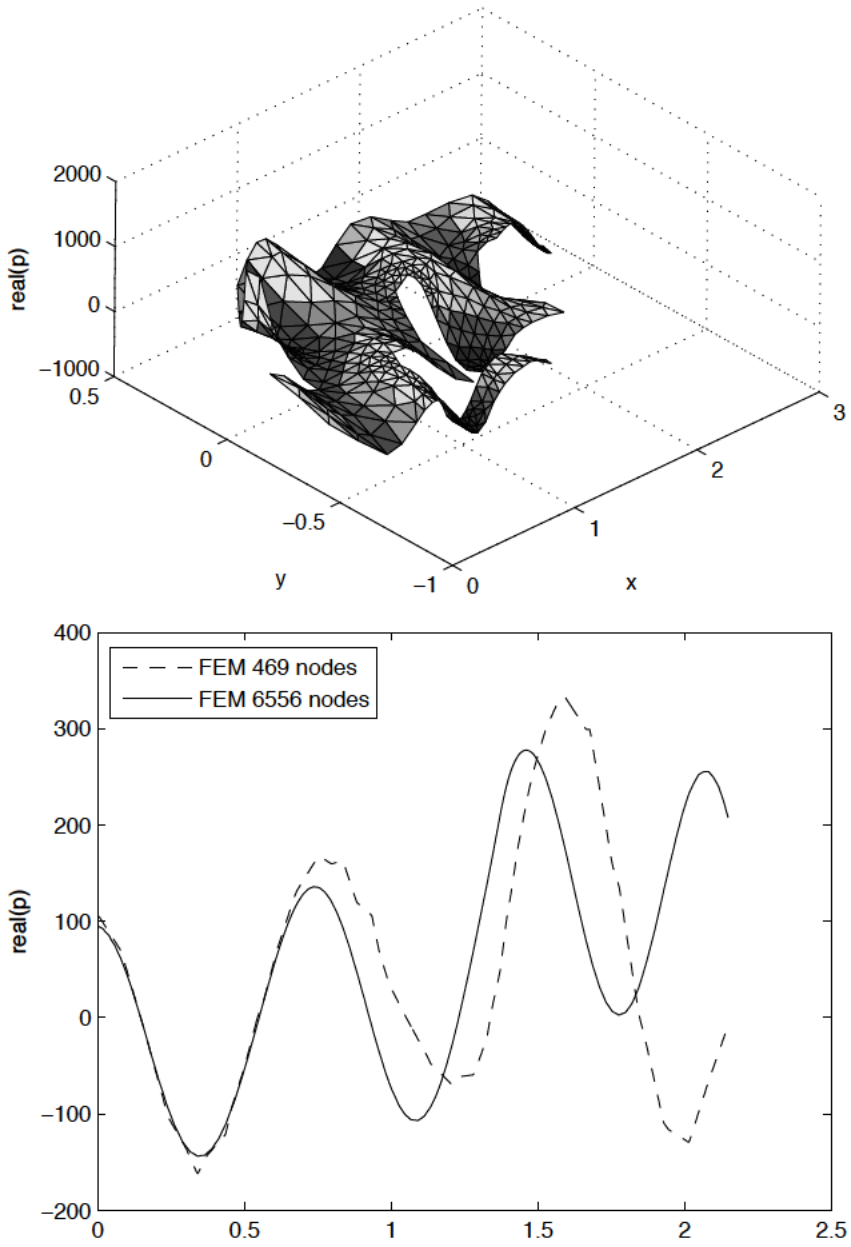

Fig. 15. *Example 3: Solution of the pressure field (top) and dispersion effect (bottom) for 525 Hz.*

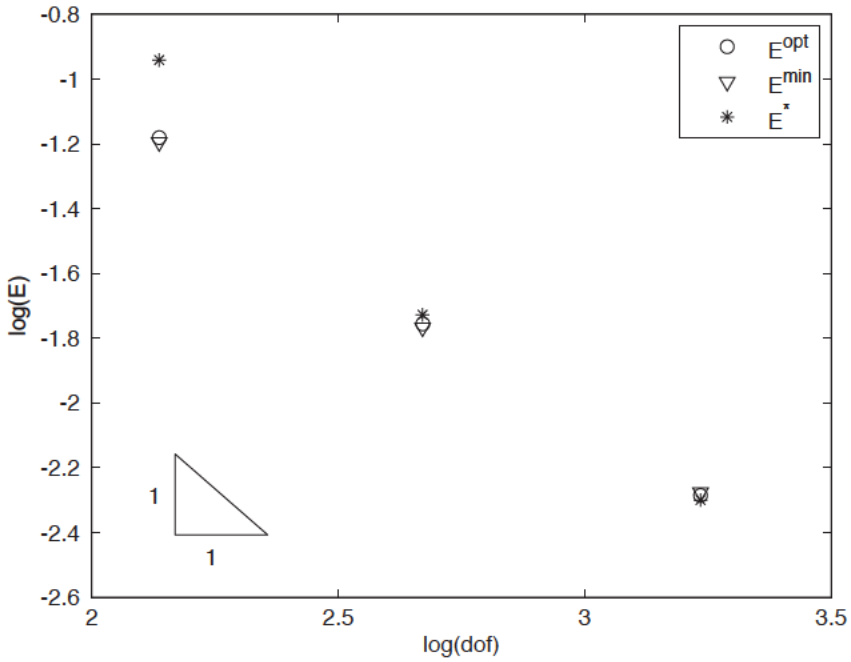

Fig. 16. Example 3: Convergence of the error.

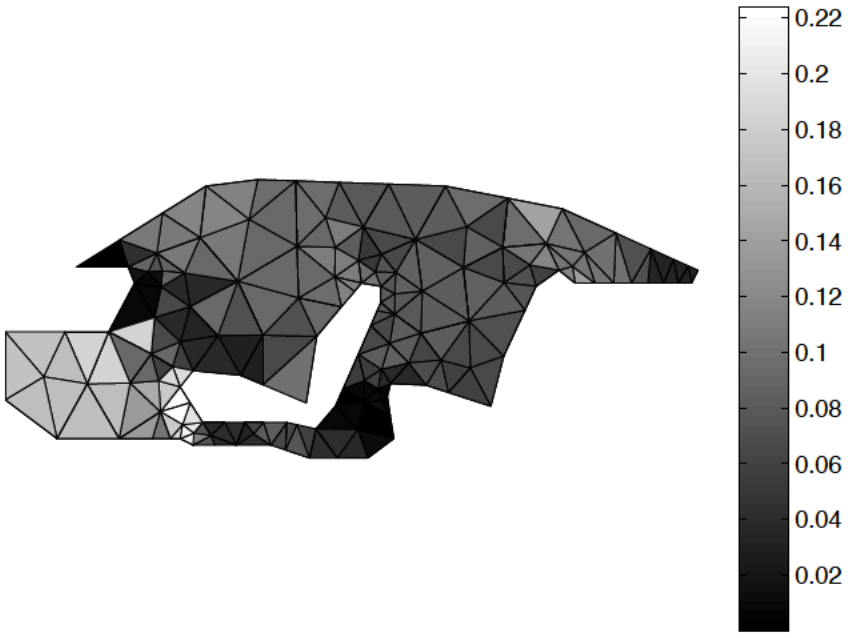

Fig. 17. Example 3: Map of the error for the car cavity problem in an mesh unstructured triangular of 137 dof.